JOURNAL OF MATERIALS SCIENCE 31 (1996) 949–955

# Preparation and sintering behaviour of submicronic $Bi_4Ti_3O_{12}$ powders

M. VILLEGAS, C. MOURE, J. F. FERNANDEZ, P. DURAN
*Instituto de Cerámica y Vidrio (CSIC), Electroceramics Department, 28500 Arganda del Rey, Madrid, Spain*

Submicronic powders of $Bi_4Ti_3O_{12}$ with different morphologies were prepared by both the oxalate coprecipitation and the conventional mixing oxides methods. Compacts of the two calcined powders were sintered at 850–1100 °C in air, and the densification process was studied by non-isothermal and dilatometric experiments. A rapid densification ( > 97% theoretical density) below 875 °C took place in the $Bi_4Ti_3O_{12}$ oxalate powder which was attributed to an extremely uniform pore-size distribution in the green compact. The possible formation of a transient liquid which promotes densification also was taken into account. The development of plate-like morphology in the conventional $Bi_4Ti_3O_{12}$ powder, broad pore-size distribution, and the plate-like colony formation, hindered rapid densification of the green compacts at low temperature. Microstructural development was studied; preliminary dielectric and electrical results are also reported.

## 1. Introduction

The bismuth titanate ($Bi_4Ti_3O_{12}$) belongs to the Aurivilius compounds family that can be described by the general formula $Bi_2O_2^{2+}(A_{m-1}B_mO_{3m+1})^{2-}$ in which A and B are cations and $m$ corresponds to the number of perovskite-type units between the bismuth oxide layers. In the particular case of the $Bi_4Ti_3O_{12}$ layer compound, its structure is formed by two $BiTiO_3$ unit cells of hypothetical perovskite structure interleaved with $Bi_2O_2^{2+}$ layers [1]. At room temperature, $Bi_4Ti_3O_{12}$ presents a monoclinic ($C_{1h}$ = m) symmetry, and above the Curie temperature (~675 °C) the symmetry is tetragonal $D_{4h}$ = 4mmm. At this temperature a reversible α–β transformation takes place and the compound is characterized by ferroelectric properties. The vector of major spontaneous polarization lies in the perovskite plane, i.e. in the monoclinic *ac* plane, and the vector intensity values of spontaneous polarization are 50 and 4 $\mu C\,cm^{-1}$ along axes *a* and *c*, respectively [2, 3]. In the same way, the piezoelectric coefficient is relatively high along these directions and small in the perpendicular plane. All the above-mentioned characteristics make $Bi_4Ti_3O_{12}$ compound of particular importance as a piezoelectric ceramic material for high temperature applications.

As reported by several authors [4–8] optimized piezoelectric properties are achieved by almost complete alignment of the plate-like bismuth titanate particles, and different techniques, such as tape casting, hot pressing and forging, were used to obtain well grain-oriented $Bi_4Ti_3O_{12}$ materials [9–12]. This being so, the main problem with these bismuth titanate-based ceramics is their extremely high electrical conductivity anisotropy which is also maximum in the basal plane [6, 9]. Such an anisotropy increases with temperature and reaches a maximum ratio near the transition temperature in $Bi_4Ti_3O_{12}$ single crystals [13]. Given that both the piezoelectric properties and the electrical conductivity are maximized in the same directions, then a well grain-oriented $Bi_4Ti_3O_{12}$ ceramic material could be unsuitable for high-temperature applications.

Because the mechanism of electrical conductivity seems to be associated with the presence of oxygen defects in the form of anionic vacancies in the $Bi_2O_2^{2+}$ layers [14], new attempts for increasing the resistivity of these bismuth titanate-based ceramics could be (a) to obtain low-temperature well-densified $Bi_4Ti_3O_{12}$ ceramics with randomly oriented small grain size which would contribute to the hindrance of the easy path conductivity in $Bi_2O_2^{2+}$ layers, and (b) to study different additives and sintering schedules for controlling both the oxygen vacancies concentration and the microstructure. The main goal of the present work was to study the influence of the $Bi_4Ti_3O_{12}$ powder morphology on its densification process and microstructural development. On that basis, some preliminary dielectric and electrical conductivity measurements also are given.

## 2. Experimental procedure

In order to obtain $Bi_4Ti_3O_{12}$ powders with different morphologies, two preparation methods were used. One of them used the unconventional oxalate preparation method, and the other one the conventional mixing of oxides. In the first method a titanium tetrabutoxide, $Ti(But)_4 \cdot C_4H_9OH$ and $Bi(NO_3)_3 x H_2O$ as $TiO_2$ and $Bi_2O_3$ precursors, respectively, were used. Stoichiometric amounts of both precursors were

0022–2461 

dissolved in a slightly acid isopropyl alcohol solution and then were added to a 0.3 M aqueous oxalic acid solution by dropping. A good coprecipitation of the oxalates was achieved by a careful pH control, and a small amount of aqueous $OH(NH_4)$ was added at the end of the coprecipitation process. The coprecipitate was thoroughly washed with isopropanol until an amorphous powder was obtained. After drying, the powder was calcined at 750 °C for 1 h and attrition milled for 2 h in an isopropanol medium. The calcined powder was granulated and isostatically pressed at 200 MPa. The compacts were sintered at 850–1100 °C for 2 h. The densification process was also studied by dilatometry in a (DI-24 Adamel-L'homargi) dilatometer.

Both the coprecipitated and the calcined powders were characterized by specific surface area measurements by using the BET method with nitrogen as the adsorbate (Micromeritics Accusorb 2100E model), a (Coulter LS 130 model) particle-size analyser, a differential thermal analyser (STA409 Nescht model), an X-ray diffractometer (D-5000 Siemens model), and a scanning electron microscope (DSM950 Karl Zeiss model).

The density of the sintered compacts was measured by the Archimedes' method with water, and the pore-size distribution and the pore volume in the green compacts were calculated by mercury porosimetry using a (Micromeritics Autopore II 9215 model) porosimeter. The microstructure of both the green and the sintered compacts was studied by SEM.

Dielectric and electrical characterization was carried out by using a HP-4192A impedance analyser in the temperature range 25–600 °C.

For comparison, a $Bi_4Ti_3O_{12}$ powder was prepared by mixing stoichiometric amounts of $TiO_2$ (Rhone Poulenc) and $\alpha$-$Bi_2O_3$ (Riedel) and calcined at 800 °C for 1 h. After attrition milling for 2 h and drying, the powder also was granulated, isostatically pressed, and sintered under the same conditions as the unconventional powder. The $Bi_4Ti_3O_{12}$ powder obtained by the unconventional method will be referred to as BIT (A) and that of the conventional one BIT (B).

## 3. Results and discussion

### 3.1. Powder characteristics

As shown in the micrograph of the Fig. 1, the coprecipitated BIT (A) powder was formed by agglomerates of particles with a size less than 50 nm and a specific surface of 25 $m^2g^{-1}$ as determined by BET. Differential thermal analysis of this powder showed two exothermic effects at 244 and 756 °C, and two endothermic ones at 515 and 650 °C, see Fig. 2. The first exothermic effect, between 200 and 400 °C, was due to both the combustion of the residual isopropanol, and the oxalate decomposition. In this temperature interval the main weight loss of the coprecipitate took place. The second exothermic effect could be due to the formation of the $Bi_4Ti_3O_{12}$ compound. The two endothermal effects were probably due to the loss of some hydroxyl groups and the $\alpha$–$\beta$ transformation of an incipiently formed $Bi_4Ti_3O_{12}$, respectively.

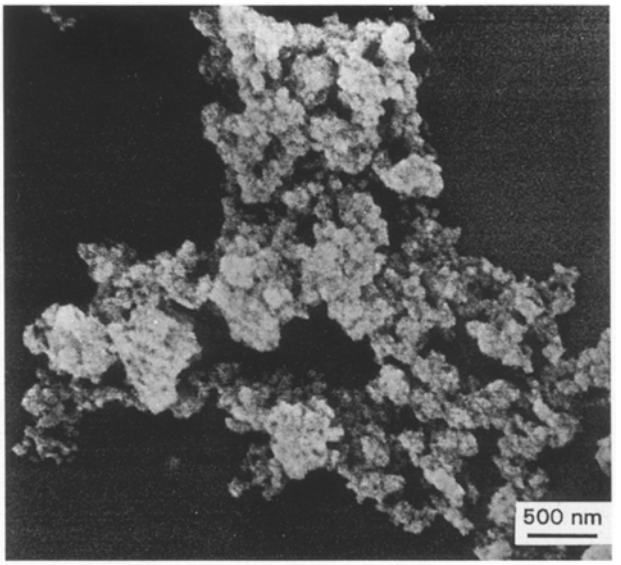


*Figure 1* Coprecipitate oxalate BIT (A) powder.

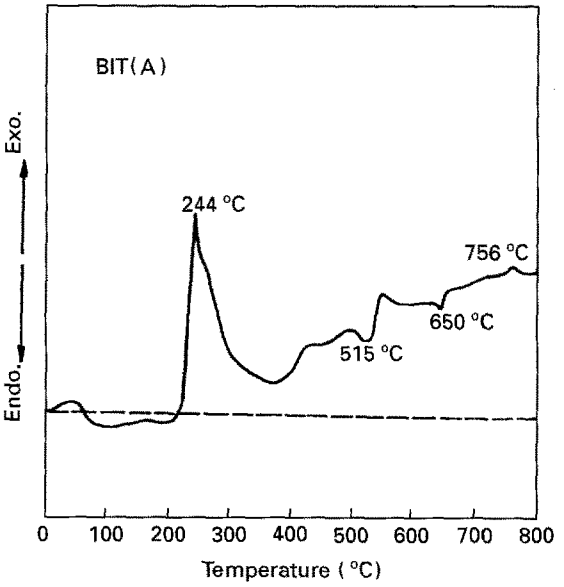


*Figure 2* DTA curve of BIT (A) powder.

After calcining and attrition milling, BIT (A) and BIT (B) powders consisted of soft agglomerates of almost equiaxed shape particles or strong spherical agglomerates with ultimate average particle sizes of 0.6 and 0.4 μm, respectively, see Fig. 3. The specific surface of the BIT (A) and BIT (B) powders were 2 and 2.4 $m^2g^{-1}$, respectively. It must be mentioned that some initial sintering seemed to take place during the calcination, and the XRD analysis of both kinds of calcined powders indicated the presence of a unique $Bi_4Ti_3O_{12}$ phase. Apparently neither platelets nor needle-like particles were developed during the calcination of the two powders. After compaction the density of the green compacts were 55% and 68% theoretical, for BIT (A) and BIT (B), respectively, and the pore-size distribution curves, as shown in Fig. 4, showed an almost single and narrow pore-size distribution for BIT (A) and a bimodal one for BIT (B). The average pore diameters were 0.1 and 0.09 μm, respectively.

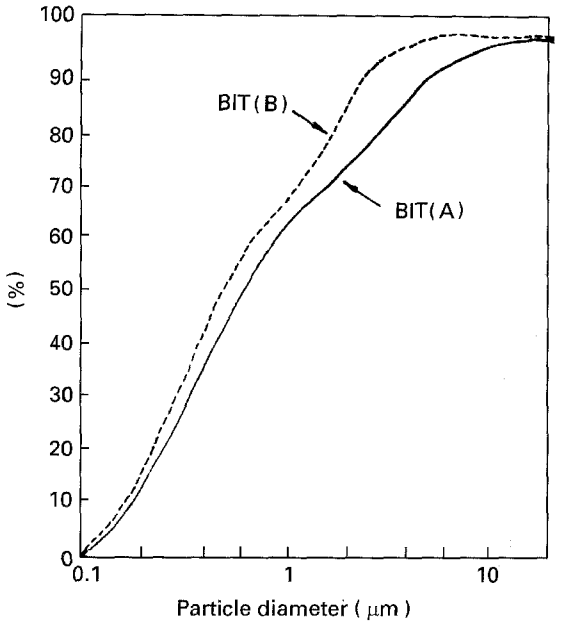


*Figure 3* Particle-size distributions of BIT (A) and BIT (B) calcined powders.

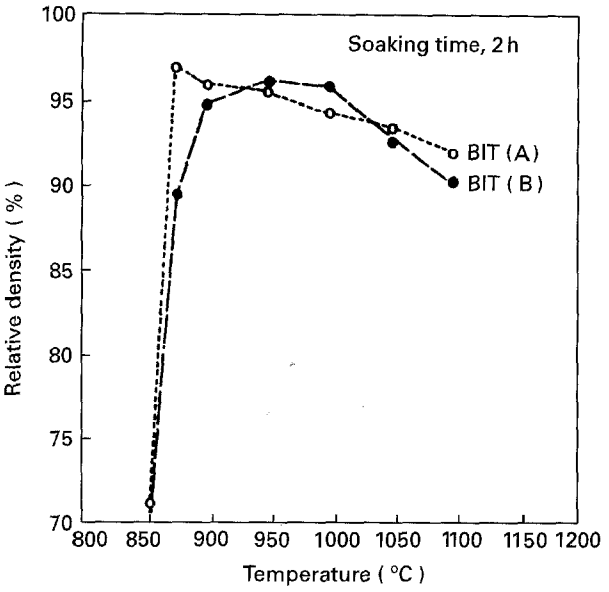


*Figure 5* Densification behaviour of BIT (A) and BIT (B) compacts.

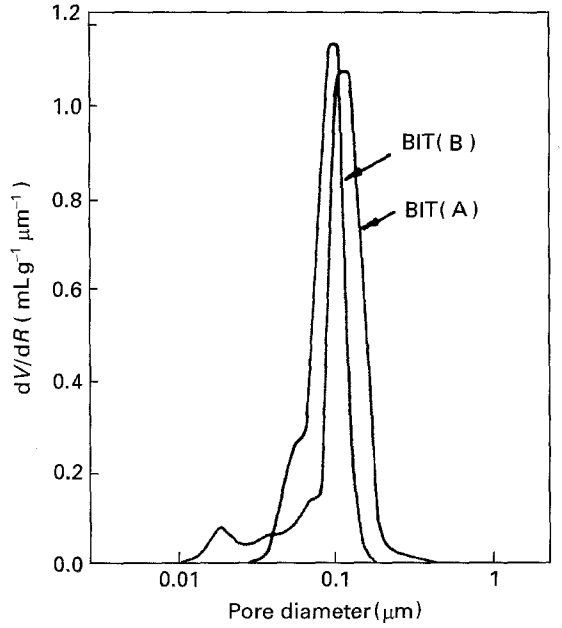


*Figure 4* Pore-size distributions in BIT (A) and BIT (B) green compacts.

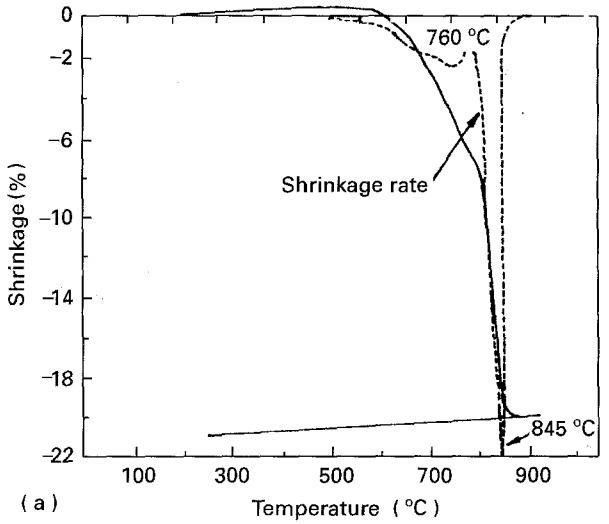


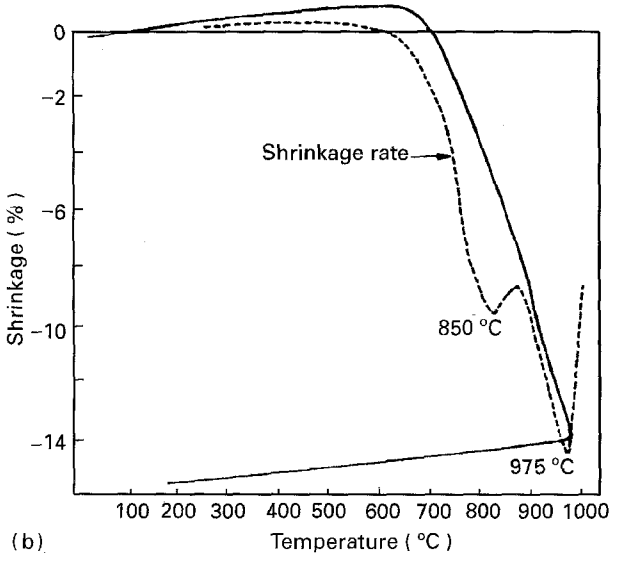


*Figure 6* Shrinkage and shrinkage-rate curves of (a) BIT (A) and (b) BIT (B) compacts.

## 3.2. Sintering

Green compacts of BIT (A) and BIT (B) were fired at 850–1150 °C for 2 h. Fig. 5 shows the effect of sintering temperature on the densification of both kinds of powder compacts. Although the temperature dependence in both cases was similar, BIT (A) compacts densified at a temperature almost 100 °C lower. The maximum densities were achieved for sintering temperatures of 875 and 950 °C for BIT (A) and BIT (B), respectively. The densification of BIT (A) compacts took place rapidly in a narrow temperature interval, between 850 and 875 °C, and above that temperature the density slightly decreased. In the case of the BIT (B) compacts, the densification process was slower, taking place in a broader temperature interval,

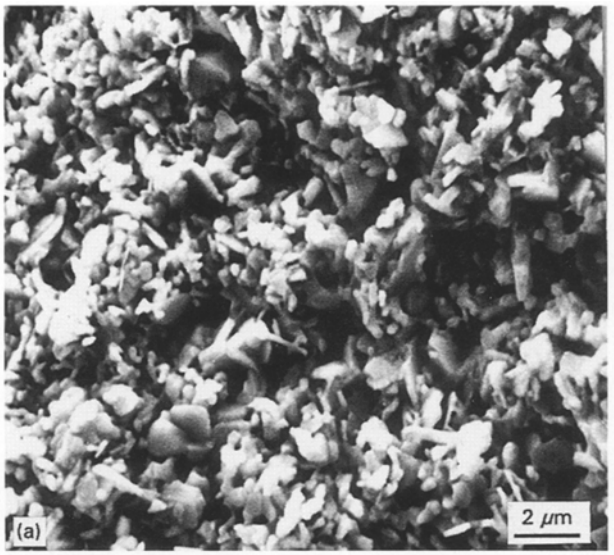


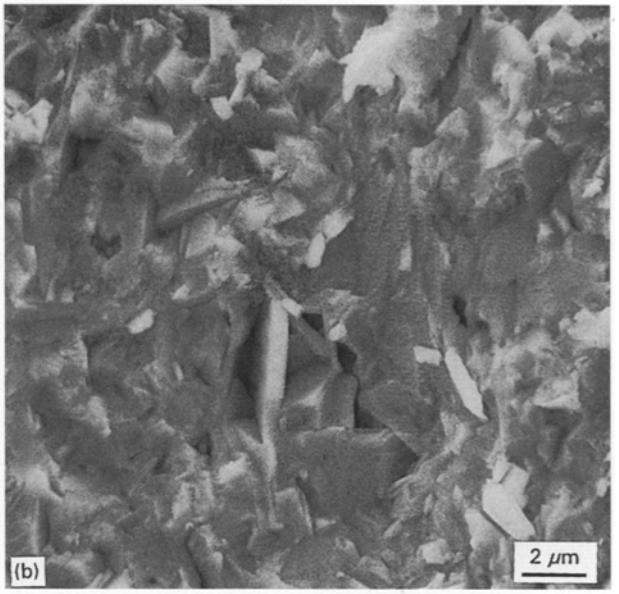


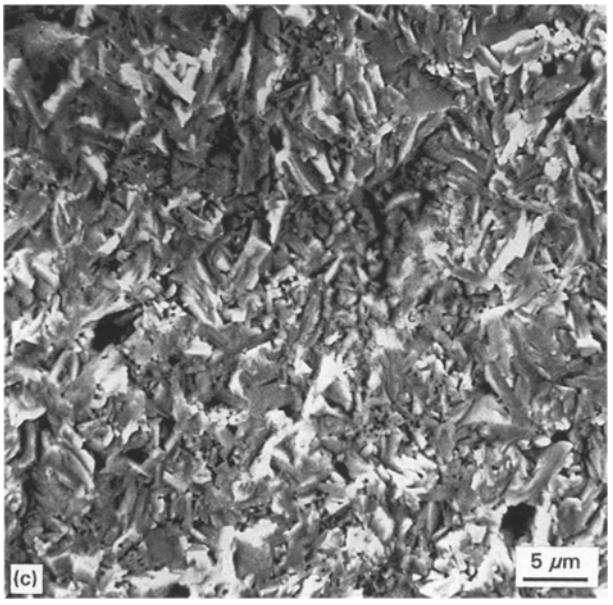


*Figure 7* Fracture surface of BIT (A) samples sintered at (a) 850 °C, (b) 875 °C, and (c) 900 °C.

between 850 and 950 °C, decreasing the density for higher temperatures.

The densification process also was studied by constant-rate heating (CRH) experiments. As shown in Fig. 6a and b, BIT (A) compact starts to shrink at a temperature as low as 600°C and an end point was reached at 875 °C for a shrinkage of about 21%. The shrinkage-rate curve showed two maxima, one at about 750 °C and the other one at approximately 860 °C. Above those temperatures the shrinkage rate decreased slightly.

In the case of BIT (B) compacts, the shrinkage started at about 750 °C, and no end point was reached below 1000 °C at which temperature a shrinkage of about 15% was produced. The shrinkage-rate curve also presented two maxima at 850 and 980 °C. Above 850 °C the shrinkage rate decreased slightly, and then increased again to reach the second maximum at 980 °C.

### 3.3. Microstructural development

A detailed study was made of the microstructure evolution with temperature for BIT (A). Fig. 7 shows the surface fracture of BIT (A) samples sintered at 850, 875 and 900 °C. At the lower temperature, randomly oriented grains with some developed plates or needles were observed. The porosity was located mainly on grain boundaries, and no pores were located in the interior of the grains or plates. The grain size, less than 1 μm, indicated that no appreciable grain growth was produced at this sintering temperature. In the sample sintered at 875 °C, a rearrangement of both the grains and/or plates with the virtual disappearance of the porosity took place. This rearrangement phenomenon coincides with the maximum of the density reached at this temperature, see Fig. 5. The few developed plates were ~0.5 μm thick and ~2 μm diameter. With further increase in temperature, many spherical pores were developed, and a rapid grain growth in the sample sintered at 900 °C was observed. Thus, the plate-like grains were ~1 μm thick and ~5 μm diameter. At higher temperatures, spherical pores located in the interior of the plate-like grains and non-spherical or triangular pores located between them, were observed. As a consequence, many cracks were also produced and, therefore, a decrease in density. Fig. 8 shows the microstructure of the BIT (A) polished surfaces and thermally etched samples sintered at 950 and 1000 °C.

In the case of the BIT (B) sintered samples the microstructure was only studied in the sample with the highest density. Fig. 9a shows the microstructure of a BIT (B) polished and thermally etched sample sintered at 1000 °C for 2 h, in which colonies of plate-like grains of ~2 μm thick and higher than 10 μm diameter, were developed. Despite the use of a

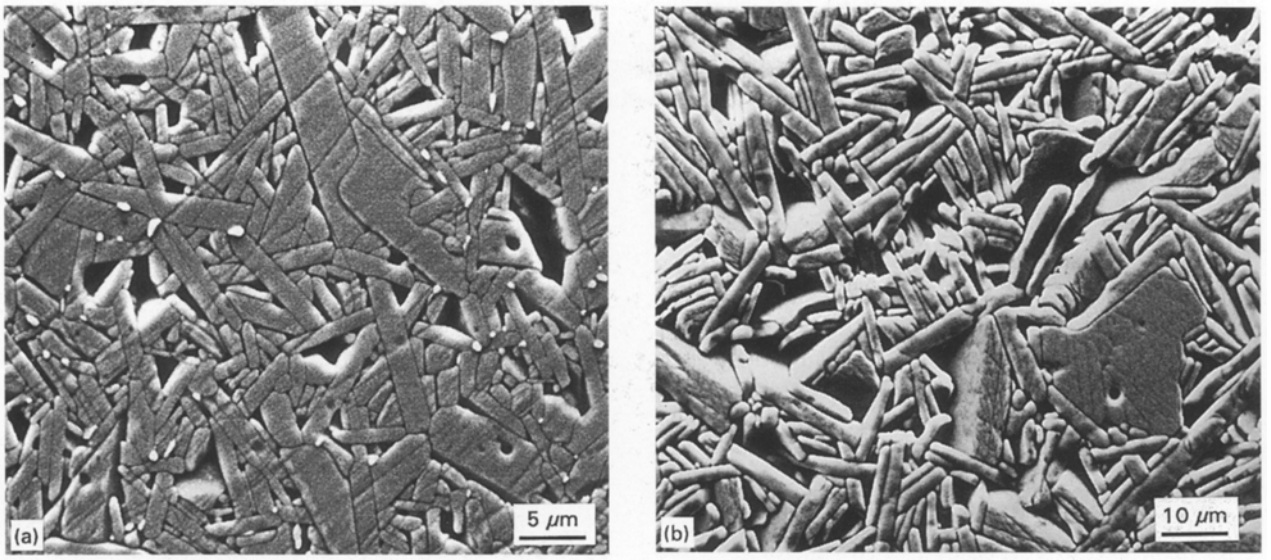


*Figure 8* Microstructure of polished and thermally etched BIT (A) samples sintered at (a) 950 °C and (b) 1000 °C.

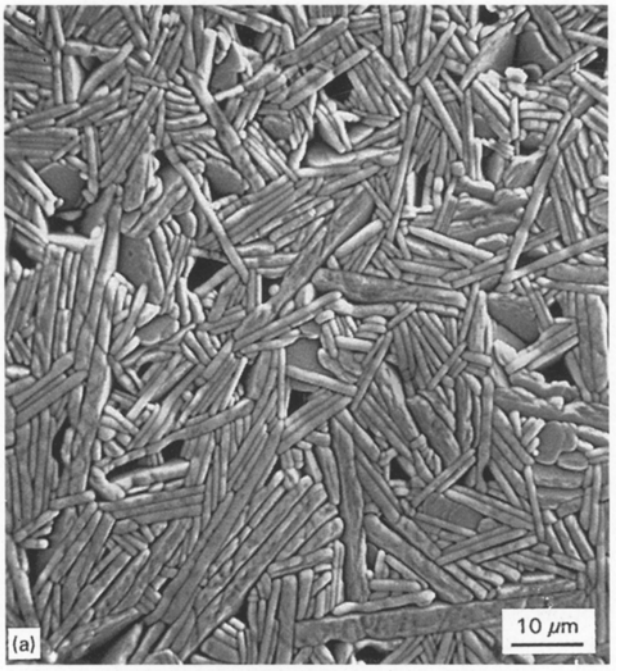


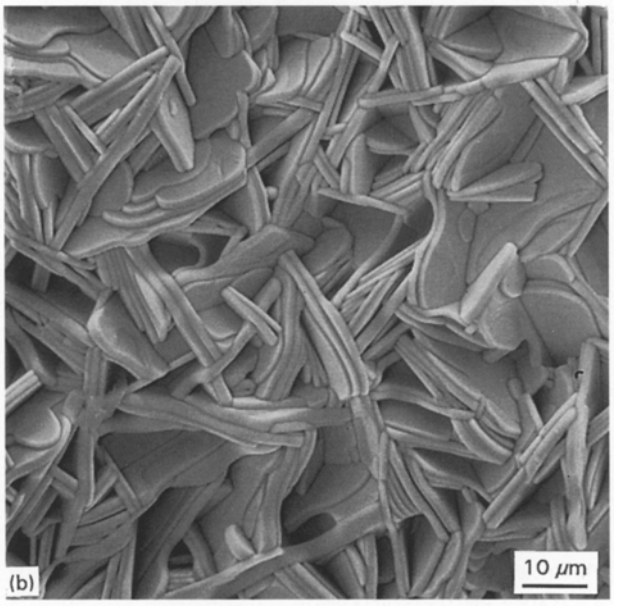


*Figure 9* Microstructure of (a) polished and thermally etched surface and (b) fracture surface of BIT (B) samples sintered at 1000 °C.

pressureless sintering process, a certain orientation degree of the plate-like bundles can be observed. Triangular-shaped pores between the plate-like colonies were developed. Fig. 9b shows the fracture surface of the same sintered sample in which a randomly oriented plate-like deformed bundle is clearly observed.

### 3.4. Dielectric properties

The dielectric constants of BIT (A) and BIT (B) sintered samples were measured at room temperature and, depending on the sintering temperature, the dielectric constant values ranged from 180–140 and from 170–125 for BIT (A) and BIT (B) samples, respectively, which indicated some influence of the grain size. It must be noted that the dielectric constant values for the denser samples were 180 and 125 for BIT (A) and BIT (B), respectively. The bulk conductivity measured at 250 °C was within the same order of magnitude, $7.8 \times 10^{-6}$ and $2.1 \times 10^{-6}\ \Omega^{-1}\text{cm}^{-1}$ for BIT (A) and BIT (B) samples, respectively.

## 4. Discussion

The sintering behaviour of BIT (A) and BIT (B) compacts strongly depends on the morphology of the $Bi_4Ti_3O_{12}$ particles. Thus the sintering behaviour of BIT (A) powder with equiaxed shaped particles was quite different to BIT (B) with incipient plate-like particles. In both cases the calcined powders were formed by aggregates of different sizes and shapes but the primary particle was smaller than 1 μm, see Fig. 3. In the case of BIT (B), spherical agglomerates without breaking remained after attrition milling which probably indicates an incipient sintering during the calcination process. In spite of a lower green density the BIT (A) compacts densified at a temperature lower than that for BIT (B) ones. Thus a maximum density of 97.5% was achieved at 875 °C for BIT (A), and only ~96% density was reached at 950 °C in the case of BIT (B), see Fig. 5. A rapid densification occurred in a temperature interval as narrow as 25 °C in the case

of BIT (A) compacts, and a rather slow densification process was present for BIT (B). For higher temperatures, the density decreased in both cases. Although no liquid formation was detected at 875 °C, it would be reasonable to think that small deviations of the stoichiometric $Bi_4Ti_3O_{12}$ composition could be present and, if this is so, then the presence of a small transient liquid amount will coexist with the $Bi_4Ti_3O_{12}$ compound above 860 °C according to the $Bi_2O_3$–$TiO_2$ phase diagram [15], and the fast densification process could thus be explained. A deeper study of the microstructure by TEM will help to elucidate this. If a transient liquid was not formed, then the rapid densification could be attributed to the very uniform pore-size distribution in the green starting compact, see Fig. 4. The steep shrinkage curve, as shown in Fig. 6a, could also support such an assumption [16].

As presented in Fig. 8a and b, two maxima in the shrinkage-rate curves were registered, and the temperature difference between them was 85 and 125 °C for BIT (A) and (B), respectively. At the two lower temperature maxima, 760 and 850 °C, the density of the sintered samples was less than 70% theoretical, and both maxima could be attributed to the porosity migration from the intraagglomerate to the interagglomerate pores. During this first step the finer porosity was eliminated and an increase in the volume of pores between agglomerates with a slight densification took place. Above those temperatures, a decrease of the shrinkage rate occurred in both BIT samples, and then a fast increase of the shrinkage rate between 800 and 845 °C took place in the BIT (A) sample. Such an increase in the shrinkage rate indicates a rapid elimination of the interagglomerate pores and coincided with the maximum density found in the non-isothermal sintering experiments, see Fig. 5. These facts, together with the majority of transgranular fracture of the sample sintered at 875 °C, as shown in Fig. 7, could corroborate the assumption of a combined effect of both the presence of a transient liquid at this thermal level and the extremely uniform pore-size distribution. On the other hand, no exaggerated grain growth was observed up to 875 °C, but above that temperature a rapid plate-like grain growth with the generation of an additional porosity occurred, see Fig. 8. The shape of the generated pores, leads us to assume that a rapid gas loss (oxygen ?) could be produced at high temperature. Such an additional porosity and the cracks produced as a consequence of the plate-like grain growth, led to a decrease in the density.

In the case of the BIT (B), a broader pore-size distribution in the green compacts must be assumed, see Fig. 4. In addition, as a consequence of the plate-like development and colony formation, a slower densification process takes place. The number of particles in a colony, the number of colonies, and the random colony orientation plays an important role in pore elimination and, therefore, in the densification rate. As shown in Fig. 9, the formation of both face-to-face contact between particles and the colony formation, are clear, and although pore elimination between particles can take place during the above-mentioned fact-to-face interaction, the random colony orientation could hinder the elimination of the pores between colonies and, thus, the densification process. The typical microstructure of the BIT (B) sintered samples was formed by a dense colony with a variable number of plate-like grains with triangular-shaped pores between them, see Fig. 9.

Dielectric permittivity measurements carried out in the denser samples of BIT (A) and BIT (B) showed a higher dielectric permittivity in the case of BIT (A). This finding could be associated with both a higher oxygen defect concentration [13] and a different microstructure. If this is so, the higher bulk conductivity of the BIT (A) sintered samples could corroborate such an assumption.

## 5. Conclusion

Randomly oriented ceramics were fabricated by sintering anisotropic $Bi_4Ti_3O_{12}$ particles obtained by both the oxalate coprecipitation method and the mixing oxides method. The formation of almost equiaxed-shaped particles in the oxalate method favoured the densification process and, thus, high density ( > 97% theoretical) was achieved at a temperature as low as 875 °C. In the conventional method, the incipient plate-like $Bi_4Ti_3O_{12}$ particles formed during calcination, impeded a high densification rate at low temperature, and only 96% dense samples were achieved at 950–1000 °C. It is believed that both a uniform pore-size distribution in the green compact and the formation of a transient liquid favoured the rapid densification of oxalate $Bi_4Ti_3O_{12}$ prepared powders above 850 °C, and a broader pore-size distribution, the formation of plate-like $Bi_4Ti_3O_{12}$ colonies and their arrangement, hindered a rapid densification below 950 °C in the conventional $Bi_4Ti_3O_{12}$ powders. In both cases, a rapid grain growth with randomly oriented grains above the maximum densification temperature gave rise to a decrease in density. Preliminary dielectric and electrical results indicate the strong influence of the microstructure, and it is suggested that different sintering schedules and doping be carried out to control exaggerated grain growth.

## References


1. B. AURIVILIUS *Ark. Kemi* **1** (1949) 499.
2. J. I. DORRIAN, R. E. NEWNHAM and D. K. SMITH *Ferroelectrics* **3** (1971) 17.
3. G. W. TAYLOR, S. A. KENEMAN and A. MILLER, *ibid.* **2** (1971) 11.
4. K. SHOJI and Y. UEHARA, *Jpn J. Appl. Phys.* **22**, *Suppl. 22-2* (1983) 50.
5. T. TAKENAKA and K. SAKATA, *ibid.* (1983) 53.
6. *idem, J. Appl. Phys.* **55** (1984) 1092.
7. T. TAKENAKA, K. SAKATA and K. TODA, *Jpn J. Appl. Phys.* **24** *Suppl. 24-2* (1985) 730.
8. Y. INOUE, T. KIMURA and T. YAMAGUCHI, *Am. Ceram. Soc. Bull.* **62** (1983) 704.
9. Y. INOUE, T. KIMURA, T. YAMAGUCHI, K. NAGATAM and K. OKAZAKI, *Yogyo Kijokaishi* **92** (1984) 416.
10. H. WATANABE, T. KIMURA and T. YAMAGUCHI, *J. Am. Ceram. Soc.* **72** (1989) 289.
11. T. TAKENAKA, K. SHOJI, H. TAKAI and K. SAKATA, in "Proceedings of the 19th Japan Congress on Materials

Research", Tokyo, Japan, March 1976, pp. 230–33.
12. H. WATANABE, T. KIMURA and T. YAMAGUCHI, *J. Am. Ceram. Soc.* **74** (1991) 139.
13. A. FONSKOVA and L. E. CROSS, *J. Appl. Phys.* **41** (1970) 2834.
14. E. V. SINJAKOV, E. F. DUDNIK, V. M. DUDA, V. A. PODOLSKI and M. A. GORFUNKEL, *Fiz. Tverd. Tela* **16** (1974) 1515.
15. E. I. PERANSKAYA, I. S. REZ, L. V. KOZLOVA and V. M. SKORIKOV, *Izv. Akad. Nauk. SSSR Neorgan Materialz.* **1** (1965) 232.
16. T. YAMAGUCHI and H. KOSHA, *J. Am. Ceram. Soc.* **5** (1981) C-84.

*Received 23 September 1994*
*and accepted 22 June 1995*